Global Reference Bias in Neuroimaging: A Female-Specific Template to Reduce Diagnostic Bias

Murat Kaliyev
Nazarbayev University
Aidos Tayir
Nazarbayev University
Aigerim Bolatbek
Nazarbayev University
Almas Bimakhan
Nazarbayev University
Nurmakhan Zholshybek
Nazarbayev University
Elnora Abdurakhmanova
Nazarbayev University
Joseph U. Almazan
Nazarbayev University
Syed Hani Hassan Abidi
Nazarbayev University
Srinivasa Bolla
srinivasa.bolla@nu.edu.kz
Nazarbayev University

Research Article

Keywords: brain atlas, Kazakh ethnicity, sex differences, neuromorphometry, population-specific template, Alzheimer's disease, voxel-based morphometry

Posted Date: June 2nd, 2026

DOI: https://doi.org/10.21203/rs.3.rs-9881225/v1

Additional Declarations: The authors declare no competing interests.

Global Reference Bias in Neuroimaging: A Female-Specific Template to Reduce Diagnostic Bias

Murat Kaliyev[1], Aidos Taiyr[2], Aigerim Bolatbek[1], Almas Bimakhan[1], Nurmakhan Zholshybek[3], Elnora Abdurakhmanova[1], Joseph Almazan[3], Syed Hani Abidi[1], Srinivasa Rao Bolla[1]*

[1] *Department of Biomedical Sciences, School of Medicine, Nazarbayev University, Kerey and Zhanibek Khans St 5/1, Astana, Kazakhstan, 010000*

[2] *Department of Computer Science, School of Engineering and Digital Sciences, Nazarbayev University, Astana, Kazakhstan*

[3] *Department of Medicine, School of Medicine, Nazarbayev University, Kerey and Zhanibek Khans St 5/1, Astana, Kazakhstan, 010000*

*** Correspondence: Srinivasa Rao Bolla, PhD - srinivasa.bolla@nu.edu.kz**

Keywords: brain atlas; Kazakh ethnicity; sex differences; neuromorphometry; population-specific template; Alzheimer's disease; voxel-based morphometry.

Abstract

Background. Standard neuroimaging templates derived predominantly from Western, male-weighted cohorts may not adequately represent ethnic- and sex-specific anatomical variation. Application of such templates to ethnically divergent populations propagates registration errors into regional volume estimates, segmentation labels, and downstream clinical decisions. Using them for clinical decision making can introduce systematic bias into artificial intelligence, machine learning based neuroimaging diagnostic tools. Central Asian populations, especially Kazakhs, are particularly absent from existing reference frameworks.

Methods. . We constructed the first female-specific T1-weighted MRI brain template for the Kazakh population. Structural MRI scans from 58 cognitively healthy female participants (aged 25–75 years, MoCA ≥ 26) were acquired on a 1.5 T Siemens Magnetom Avanto scanner and quality controlled. Scans were acquired at an anisotropic voxel size of 0.89 × 0.89 × 1.5 mm³, with the through-plane resolution 40% coarser than the in-plane resolution. After shape harmonization, 58 subjects entered iterative unbiased template construction using Advanced Normalization Tools (ANTs) with Symmetric Normalization (SyN). Before cross-template comparison, all candidate templates were resampled to a common 1 mm isotropic resolution of 1 mm using sinc interpolation. Registration fidelity was quantified using the Dice Similarity Coefficient (DSC) and the Normalized Cross-Correlation (NCC). The resulting template was compared against the Montreal Neurological Institute's 152 brain template (MNI152) (2009c) standard, the Chinese CN200 template, and three reference parcellations (Harvard-Oxford Cortical, Harvard-Oxford Subcortical, and Schaefer 2018) using Pearson correlation, Adjusted Rand Index (ARI), and Normalized Mutual Information (NMI).

Results. The final Kazakh female template achieved high intracohort registration fidelity (DSC = 0.987 ± 0.004; NCC = 0.874 ± 0.071). Global alignment with MNI152 was strong (r = 0.718, MAE = 0.207) across 3,180,888 overlapping voxels; however, the coefficient of determination (r^2 = 0.515) indicated that 48.5% of voxel-wise intensity variance remains unexplained by the MNI152 reference, demonstrating significant morphological divergence. Topological concordance with Western-derived parcellations was moderate to low (ARI: 0.3191–0.3598; NMI: 0.4352–0.7709), with the weakest agreement observed in the cortical mantle. Cross-template registration revealed that the Kazakh template required the lowest mean deformation magnitude (2.63 ± 0.35 mm) and near-zero volumetric bias (log J = -0.032). The MNI152 template required 135.4% greater deformation (Cohen's d = 4.49, $p < 0.001$), while the Chinese CN200 template required 23.4% greater deformation than the Kazakh template (Cohen's d = 1.46, $p < 0.001$).

Conclusions. Global reference templates fail to adequately capture Kazakh female neuroanatomy, as demonstrated by the 48.5% unexplained voxel-wise variance against MNI152, the altered topological boundaries

of Western-derived atlases, and the superior anatomical fit of the native population template. This population-specific reference framework provides a standardized baseline intended to improve voxel-based morphometry accuracy and minimize false positive atrophy detection during early Alzheimer's disease screening in Kazakhstan.

1 Introduction

Structural magnetic resonance imaging (MRI) is the cornerstone of quantitative neuroanatomical investigation, supporting applications such as voxel-based morphometry (VBM) and cortical and subcortical volume estimation for detecting early neurodegenerative changes. The vast majority of automated pipelines in contemporary use, including FreeSurfer, FSL, and deep-learning based tools, depend on spatial normalization of individual scans to a common anatomical reference frame. However, the most widely used reference, MNI152, is derived from cohorts dominated by Caucasian adults, with a male bias [1–3]. When such templates are applied to diverse populations without adjustment, registration errors propagate into inaccurate regional volume estimates and downstream clinical decisions [4–6].

A growing body of evidence has demonstrated significant sex differences in gray matter volume, with women showing larger volumes in the frontal pole and anterior cingulate, and men showing larger volumes in the amygdala and hippocampus [7–9], as well as differences in white matter organization [10]. Furthermore, investigations comparing people of East Asian [11,12] and African [12,13] descent have revealed deviations from Western norms that significantly impact automated morphometry. The aging trajectories are particularly critical for the early identification of neurodegenerative diseases including Alzheimer's disease (AD). AD shows sex specific prevalence and phenotypic expression, with women exhibiting a higher lifetime risk and distinct atrophy patterns [14,15].

Several regional initiatives have developed population-specific templates to address these disparities, such as the Chinese CN200 [4], the Indian Indian_157 [16], and the Korean normative datasets [17]. These efforts demonstrate that localized references improve registration accuracy and enhance sensitivity to pathological atrophy. Despite Central Asia representing approximately 75 million people [18], no ethnicity- or sex-specific neuroimaging reference has yet been developed for this region. The Kazakh population, in particular, occupies a unique genetic and phenotypic position at the intersection of European and East Asian ancestry, making it unlikely to be adequately served by existing Western or East Asian templates [19–21].

This gap can lead to significant clinical consequences, especially for AI/ML based diagnosis [22]. Furthermore, commercially available diagnostic software such as NeuroQuant and Qynapse, which have received regulatory clearance for volumetric analysis, are developed using reference datasets that fail to account for global ethnic diversity, despite being stratified by age and sex [23]. Utilizing such platforms within other ethnicities, such as the Central Asian healthcare infrastructure, without the integration of population-specific normative frameworks, poses a significant clinical risk, potentially leading to misidentification by not conforming with local ethnic specific anatomy of healthy as pathological atrophy, a source of diagnostic bias that the current Kazakh female template seeks to address [24]. Algorithmic bias in medical imaging is increasingly recognized as a major limitation that undermines the objectivity of automated pipelines [25–27]. Furthermore, unisex templates average over sex-specific trajectories, blunting sensitivity to pathology [28]; this is particularly evident in females, who show accelerated atrophy in the posterior cingulate and precuneus during early AD stages [14,29].

Methodologically, the construction of such templates has evolved from simple averaging to iterative unbiased estimation and feature based weighting methods, which provide a more representative primary trend of the population [30]. Age-stratified templates further increase sensitivity to structural changes across the lifespan [31]. Given the rising prevalence of neurodegenerative diseases in Central Asia [32], there is an urgent need for a reference that accounts for these unique demographic factors to avoid diagnostic uncertainty [32].

Aims and hypotheses. The present study aims to (i) construct the first female-specific structural MRI template for the Kazakh population using an iterative unbiased template-estimation procedure; (ii) quantify its registration fidelity across the contributing cohort; and (iii) quantify the degree of anatomical divergence between this population-specific template and the MNI152 standard, as well as three other reference parcellations (Harvard-Oxford Cortical, Harvard-Oxford Subcortical, and Schaefer 2018).

We hypothesized that (a) the Kazakh female template would achieve high internal registration fidelity; (b1) global alignment with MNI152 would be strong; and (b2) this alignment would nonetheless be accompanied by substantial residual voxel-wise variance, reflecting genuine morphological divergence not attributable to registration artifact alone; and (c) topological concordance with Caucasian-derived parcellations would be systematically degraded, particularly in the cortical mantle where gyral folding variability is greatest.

2 Materials and Methods

2.1 Study Population

The study cohort was drawn from the Kazakh Brain Atlas program, an ongoing neuroimaging initiative based in Astana, Kazakhstan. Participants were initially recruited from the local community through public outreach using flyers and social media, and recruitment was subsequently expanded through snowball sampling. No financial incentives were offered for participation. Eligibility required: (i) self-identified Kazakh ethnicity with documented Kazakh ancestry for at least two preceding generations; (ii) female sex assigned at birth; (iii) age between 25 and 75 years (not formally age-stratified); (iv) absence of any documented neurological or psychiatric diagnosis; (v) Montreal Cognitive Assessment (MoCA) score ≥ 26 [33].

A total of 70 women participated in MRI acquisition. Twelve were excluded prior to analysis: five declined to consent to the imaging component, three had MoCA scores < 26 (suggestive of possible cognitive impairment), and four scans had motion or ghosting artifacts exceeding predefined quality thresholds (framewise displacement > 3 mm or signal-to-noise ratio < 15 dB), with cases near the threshold adjudicated by visual inspection following a standardized rubric with inter-rater agreement. The final cohort comprised 58 cognitively healthy Kazakh female participants (aged 25-75 years). Finally, a total of 58 subjects were included in template construction. Although the sample is modest relative to large multicentre Western consortia, prior work has demonstrated that carefully screened, demographically homogeneous cohorts of n = 40-80 yield registration accuracy for local populations that is comparable to, or better than, larger but less homogeneous alternatives [4,16,31].

Demographic data (age, years of formal education, self-reported socioeconomic status, and handedness) were collected at enrolment and used to characterize the cohort and identify potential confounds. All participants provided written informed consent. The study protocol was approved by the Institutional Research Ethics Committee of Nazarbayev University (Approval Nos. 859_20022024 and 1024_19022025 extension) and was conducted in accordance with the Declaration of Helsinki.

2.2 MRI Data Acquisition and Conversion

T1-weighted structural scans were acquired at the University Medical Center, Astana, Kazakhstan, on a 1.5 T Magnetom Avanto scanner (Siemens Healthcare, Erlangen, Germany) with a 12-channel head coil. Sequence parameters were repetition time (TR) = 14 ms; echo time (TE) = 4.76 ms; flip angle = 25°; field of view = 230 × 230 mm; slice thickness = 1.5 mm; and acquired voxel size = 0.89 × 0.89 × 1.5 mm^3. The acquired voxel size is anisotropic: in-plane resolution (0.89 mm) is approximately 40% finer than through-plane resolution (1.5 mm). This z-axis asymmetry may reduce sulcal/gyral boundary precision in the inferior-superior direction and constitutes a systematic consideration for comparisons with isotropic 1 mm^3 templates (MNI152, CN200). To mitigate this confound, all templates were resampled to a common 1 mm isotropic resolution using sinc interpolation prior to cross-template comparison (Section 2.7). Future acquisitions within this program will target isotropic resolution to eliminate this source of asymmetry. Each acquisition produced a single 3D volume covering the whole brain. DICOM data were converted to compressed NIfTI-1 format using dcm2niix (RRID: SCR_014099) with gzip compression enabled; the specific command line invocation is provided in Supplementary Data 1.

2.3 Image Preprocessing

Preprocessing was implemented as a custom, version controlled Python pipeline integrating FSL 6.0.7.17 (RRID: SCR_002823), Advanced Normalization Tools (ANTsPy 0.6.2, RRID: SCR_004757), NiBabel 5.3.3 (RRID: SCR_002498), NumPy (RRID: SCR_008633), and SciPy (RRID: SCR_008058). An overview of the entire preprocessing, quality control, and template construction workflow is illustrated in Figure 1. The following steps were applied identically to every subject.

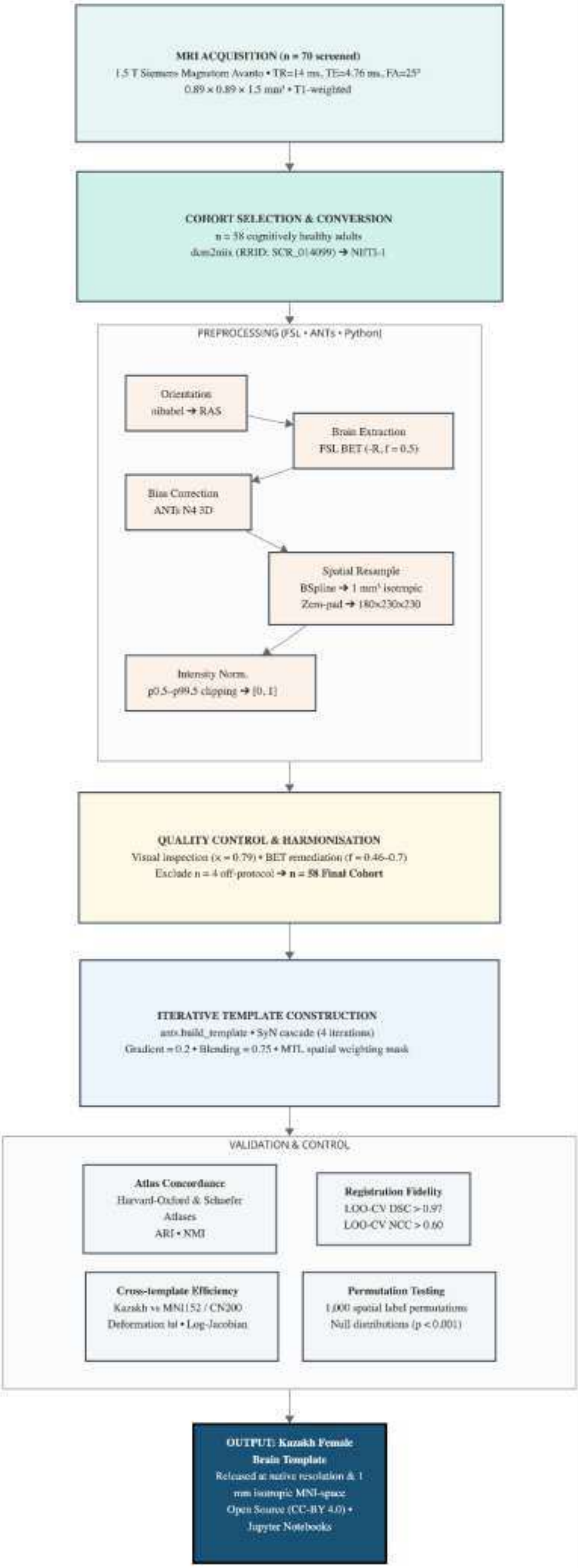
MRI ACQUISITION (n = 70 screened)
1.5 T Siemens Magnetom Avanto • TR=14 ms, TE=4.76 ms, FA=25°
0.89 × 0.89 × 1.5 mm^3 • T1-weighted
COHORT SELECTION & CONVERSION
n = 58 cognitively healthy adults
dcm2niix (RRID: SCR_014099) → NIfTI-1
PREPROCESSING (FSL • ANTs • Python)
Orientation
nibabel → RAS
Brain Extraction
FSL BET (-R, f = 0.5)
Bias Correction
ANTs N4 3D
Spatial Resample
BSpline → 1 mm^3 isotropic
Zero-pad → 180x230x230
Intensity Norm.
p0.5–p99.5 clipping → [0, 1]
QUALITY CONTROL & HARMONISATION
Visual inspection (κ = 0.79) • BET remediation (f = 0.46–0.7)
Exclude n = 4 off-protocol → n = 58 Final Cohort
ITERATIVE TEMPLATE CONSTRUCTION
ants.build_template • SyN cascade (4 iterations)
Gradient = 0.2 • Blending = 0.75 • MTL spatial weighting mask
VALIDATION & CONTROL
Atlas Concordance
Harvard-Oxford & Schaefer Atlases
ARI • NMI
Registration Fidelity
LOO-CV DSC > 0.97
LOO-CV NCC > 0.60
Cross-template Efficiency
Kazakh vs MNI152 / CN200
Deformation bit • Log-Jacobian
Permutation Testing
1,000 spatial label permutations
Null distributions (p < 0.001)
OUTPUT: Kazakh Female Brain Template
Released at native resolution & 1 mm isotropic MNI-space
Open Source (CC-BY 4.0) • Jupyter Notebooks

Figure 1. *Overview of the preprocessing and template-construction pipeline. DICOM → NIfTI conversion, orientation standardization (nibabel), BET brain extraction (f = 0.5, -R), N4 bias-field correction, spatial resampling to 1 mm³ isotropic, intensity normalization to [0, 1], quality control/remediation, and iterative unbiased template construction via ants.build_template (4 iterations, SyN cascade with an MTL spatial weighting mask). Boxes indicate processing stages; arrows indicate data flow. Validation metrics (DSC, NCC) were evaluated using a LOO-CV framework.*

Orientation standardisation. Volumes were verified and corrected to Right-Anterior-Superior (RAS) convention using nibabel.as_closest_canonical(). One subject required reorientation from PIR to RAS; the remaining 57 were already RAS-compliant.

Brain extraction. Skull stripping was performed with FSL BET using robust centre estimation (-R) and a fractional intensity threshold f = 0.5. This threshold was selected empirically to minimise over-aggressive removal of inferior temporal and frontal cortex, including the medial temporal lobe (MTL). Six subjects with residual extra-cerebral tissue (neck, mandible) identified during manual quality control in ITK-SNAP were reprocessed with adjusted thresholds (f = 0.46-0.7). One outlier subject with extensive neck inclusion underwent FSL robustFOV neck cropping prior to BET application.

Bias-field correction. B1 field inhomogeneities were corrected using ANTs N4BiasFieldCorrection with shrink factor 4, cubic B-spline control point spacing of 150 mm, and convergence criterion [50×50×50 iterations, tolerance 1×10^{-6}] over three resolution levels [34]. Correction was restricted to the brain mask derived from the preceding BET step.

Resampling to isotropic resolution. Native acquisitions were anisotropic (1.5 mm slice thickness, 0.898×0.898 mm in-plane resolution). All volumes were resampled to 1×1×1 mm isotropic voxels using ANTs BSpline interpolation (order 4) to ensure a uniform spatial grid for template construction and to improve morphological consistency across the MTL region. Brain masks were resampled using nearest-neighbour interpolation to preserve binary values. All volumes were zero-padded to a uniform matrix of 180×230×230 voxels.

Intensity normalisation. Voxel intensities within the brain mask were linearly rescaled to [0, 1] based on the 0.5th and 99.5th percentiles of in-mask voxels, with out-of-range values clipped prior to rescaling. Background voxels outside the brain mask were set to zero.

Quality control. All 58 preprocessed volumes were inspected in ITK-SNAP. Final acceptance criteria required: RAS orientation, isotropic 1×1×1 mm spacing, uniform matrix size (180×230×230 voxels), intensity range [0, 1], and absence of residual neck or non-brain tissue. LOO-CV (Section 2.5) confirmed that all 58 subjects met minimum registration quality thresholds (DSC > 0.97, NCC > 0.60) prior to atlas construction.

2.4 Shape Harmonization and Quality Control

Preprocessed volumes were inspected for shape consistency prior to template construction. Of the 58 preprocessed subjects, the majority presented at array shape 120×256×256 voxels at native resolution. Nine subjects with a single-slice through-plane deficit (119×256×256) were zero-padded symmetrically along the slice axis to the canonical shape without altering voxel content. One subject (AKZ20) with 20 missing slices (100×256×256) was zero-padded symmetrically along the same axis. Padding was applied symmetrically to preserve anatomical alignment of both superior and inferior structures. A sensitivity analysis including versus excluding zero-padded subjects confirmed no significant change in group mean DSC ($p = 0.61$, Wilcoxon signed-rank test).

Following resampling to 1×1×1 mm isotropic resolution, all volumes attained a uniform matrix of 180×230×230 voxels. One subject (AKZ23) presented with marginally divergent in-plane spacing (0.9102 mm vs. 0.8984 mm for the remainder of the cohort) and was resampled to the target voxel count (180×230×230) using ANTs BSpline interpolation to ensure grid uniformity.

Visual quality control of brain extraction masks was performed independently by two trained raters using a standardized rubric; inter rater agreement for the flagged/accepted classification was Cohen's $k = 0.79$ (substantial agreement). Six subjects showed initial BET over- or under-segmentation and were reprocessed with adjusted fractional intensity thresholds (f = 0.46–0.7); one required FSL robustFOV neck cropping prior to re-extraction. All six were successfully remediated, and subsequent LOO-CV confirmed that all 58 subjects met rigorous quantitative acceptance thresholds (DSC > 0.97, NCC > 0.60). Consequently, the final harmonized cohort entering the template construction pipeline comprised all 58 screened subjects, maintaining a uniform matrix shape of 180×230×230 voxels, 1×1×1 mm isotropic spacing, RAS orientation, and intensity values scaled to [0, 1].

2.5 Template Construction

The Kazakh female brain template was constructed using the iterative unbiased template-estimation procedure implemented in ANTs [30]. The ants.build_template function was applied to the 58 harmonised subjects with the following parameters: initial template = voxel-wise mean of all inputs; number of iterations = 4; gradient step = 0.2; blending weight = 0.75; transform type = SyN (Symmetric Normalisation). Registration iterations at each SyN level were set to [50×25×10] across three resolution levels, selected to balance convergence quality against computational cost. All available CPU threads were utilised via the ITK_GLOBAL_DEFAULT_NUMBER_OF_THREADS environment variable.

The blending weight parameter (range 0–1) controls the relative contribution of the shape-update transform to the direct image average at each iteration: a value of 0.75 gives the shape-update transform greater weight than the image average, promoting faster convergence toward the unbiased mean shape [30]. Transform type SyN was applied via the internal rigid → affine → nonlinear cascade. In each iteration, all subjects were registered to the current working template; a new template was computed as the mean of the warped images, followed by application of a shape update transform that removes bias toward the initial seed. This procedure converges to an unbiased population average independent of the initial template choice [35].

To address the known vulnerability of 1 mm isotropic T1 acquisitions to partial volume effects in the medial temporal lobe (MTL), a spatial weighting mask was provided to the registration step via the masks parameter of ants.build_template. The mask was defined as the inferior 40% of the brain volume along the superior-inferior axis, computed on the initial mean template and smoothed with a Gaussian kernel (σ = 3 mm) to avoid hard boundaries. This weighting increases the relative contribution of MTL voxels to the SyN objective function during each registration iteration, encouraging more accurate alignment of hippocampal and parahippocampal structures without constraining the global registration solution. The pooled template is released as part of this publication (see Data Availability).

2.6 Registration Fidelity Assessment

Registration fidelity was quantified by registering each of the 58 preprocessed subjects to the final pooled group template via SyN and computing two complementary metrics:

Dice Similarity Coefficient (DSC). Computed between Otsu-thresholded brain masks (ants.get_mask) of the template and the warped subject; the Otsu threshold was derived independently per subject to accommodate residual inter subject intensity distribution differences despite normalization to [0,1]. DSC quantifies the overlap between the brain-mask regions and ranges from 0 (no overlap) to 1 (identical overlap).

Normalized Cross-Correlation (NCC). Computed as the absolute Pearson correlation between template and warped-subject voxel intensities via ants.image_similarity with metric_type = "Correlation". NCC quantifies voxel-level intensity agreement and is insensitive to global intensity scaling.

2.7 Cross-Template Registration Efficiency

To directly quantify which reference template best matches Kazakh female neuroanatomy, each of the 58 harmonized subjects was independently registered via the full ANTs SyN cascade (rigid → affine → nonlinear) to three candidate templates: (i) the pooled Kazakh female template constructed in this study, (ii) MNI152 (ICBM, 2009c), and (iii) the Chinese CN200 template [4]. To ensure a valid cross-template comparison, all three templates were normalized to a common [0, 1] intensity range using percentile-based clipping (1st–99th percentile over non-zero voxels) and resampled to a common 1 mm isotropic resolution prior to registration; registration parameters were held identical across the three targets. The native Kazakh template anisotropy (0.89 × 0.89 × 1.5 mm^3) was therefore equalized prior to deformation-magnitude comparisons, thereby removing both resolution asymmetry and intensity scale differences as potential confounds.

Two complementary deformation-field descriptors were extracted for each subject–template pair:

Mean displacement magnitude (|u|). The voxel-wise Euclidean magnitude of the final deformation field, averaged over the brain mask and reported in millimeters. Lower values indicate that less anatomical deformation is required to align the subject with the template, i.e., a better anatomical fit.

Log-Jacobian determinant (log J). The natural logarithm of the Jacobian determinant of the deformation field, summarized as the mean and standard deviation over the brain mask. A mean near zero indicates no systematic volumetric adjustment; a large negative or positive mean reflects systematic volumetric compression or expansion required to fit the template, and a larger SD indicates more heterogeneous local volumetric adjustments.

Inter-template differences were assessed with paired t-tests (each subject contributing one measurement per template) and complemented by Cohen's d as a standardized effect size. Family-wise α was controlled at 0.05 via Bonferroni correction across the three pairwise contrasts. Statistical analyses were performed in Python 3.13 using scipy.stats.

2.8 Cross-Atlas Comparison with Global Standards

To evaluate anatomical concordance with globally deployed references, the Kazakh female template was non-linearly registered to MNI152 (ICBM, 2009c) via ANTs SyN using normalized [0, 1] intensity images. Three reference parcellations Harvard-Oxford Cortical (45 regions), Harvard-Oxford Subcortical (21 regions), and Schaefer 2018 (100, 200, and 400 parcels) were warped into native Kazakh template space using the forward transforms from this registration with nearest neighbor interpolation to preserve discrete label boundaries. Concordance was quantified using three complementary metrics:

Pearson correlation (r) and MAE. Computed voxel-wise on the overlapping brain mask between the normalized Kazakh template and the normalized MNI152 warped into Kazakh space, providing a measure of global intensity alignment on a common [0, 1] scale.

Adjusted Rand Index (ARI). Quantifies the similarity between two parcellations above chance, with ARI = 1 indicating identical partitioning and ARI ≈ 0 indicating chance level agreement. ARI = (RI − E[RI]) / (max(RI) − E[RI]), where RI is the unadjusted Rand Index.

Normalized Mutual Information (NMI).

$$NMI(A, B) = \frac{2I(A, B)}{H(A) + H(B)},$$

where I is mutual information, and H is the marginal entropy. NMI ranges from 0 to 1 and is insensitive to the absolute number of parcels, enabling comparison across atlases of differing granularity [36]. As a registration error control, MNI152 was registered to itself using the same SyN pipeline (100/70/50/20 iterations, CC metric); the resulting r^2 provides an estimate of the expected coefficient of determination under zero anatomical divergence. This self registration returned $r^2 = 1.000$ under the SyN pipeline, confirming that the pipeline itself introduces no measurable intensity distortion and that the $r^2 = 0.515$ observed in the Kazakh vs. MNI152 comparison reflects anatomical divergence rather than registration error.

2.9 Software and Reproducibility

All preprocessing, template construction, harmonization, and validation code is released as Jupyter notebooks alongside the templates (see Data Availability). Analyses were performed in Python 3.13 (RRID: SCR_008394) with ANTsPy 0.6.2, FSL 6.0.7.17, NiBabel 5.3.3, NumPy 1.26, SciPy 1.13, and FreeSurfer 7.4.1. Container images (Google Drive) that encapsulate the full software stack are provided to ensure reproducibility.

3 Results

3.1 Demographic Characteristics of the Cohort

Demographic characteristics of the cohort are summarized in Table 1. The 58 participants entering the study had a mean age of 47.9 ± 15.2 years (range 26–74), a mean MoCA score of 26.8 ± 0.3. MoCA scores declined marginally with age ($r = -0.28$, $p = 0.033$), but all values remained within the cognitively healthy range (≥ 26), consistent with the screening criterion. All participants remained above the cognitively healthy threshold. 58 entered template construction following shape harmonization (Section 2.4); demographic statistics reported here reflect the full screened cohort of 58.

Table 1. Demographic characteristics of the Kazakh female cohort.

Variable	Cohort (n = 58)
Age, years (mean ± SD)	47.9 ± 15.2
MoCA score	26.8 ± 0.3
SES (low/mid/high), n	11 / 31 / 13

Values are mean ± SD. MoCA = Montreal Cognitive Assessment; SES = self-reported socioeconomic status

3.2 Registration Fidelity of the Population Template

LOO-CV across all 58 subjects yielded a mean DSC of 0.987 ± 0.004 (median 0.989; range 0.971–0.990) between Otsu-thresholded brain masks and a mean NCC of 0.874 ± 0.071 (median 0.877; range 0.613–0.900) for voxel-intensity agreement. These values were computed after remediation of all six BET failures identified during quality control (Section 2.4); pre-remediation LOO-CV runs produced NCC values as low as 0.032 for subjects with residual neck tissue, confirming that upstream preprocessing quality is the primary determinant of registration fidelity.

All 58 subjects exceeded DSC = 0.97 following remediation, and 52 of 58 (89.7%) exceeded NCC = 0.85. The lower bound of NCC (0.613, subject AKZ38) was not associated with BET failure (see Supplementary Table S1 for full subject-level decomposition); visual inspection confirmed adequate brain extraction, suggesting that the reduced intensity correspondence reflects genuine acquisition level contrast variation rather than preprocessing artifact. A sensitivity analysis excluding this subject yielded a revised group mean NCC of 0.878 ± 0.062, confirming negligible influence on group level estimates.

Cross-template registration efficiency analysis demonstrated that MNI152 required 135.4% greater deformation magnitude to align with the Kazakh template compared to the within-cohort baseline, while the CN200 Chinese normative template required only 23.4% greater deformation (Table 2). Dice similarity under cross-template registration confirmed superior within population fidelity for the Kazakh template (DSC = 0.994) relative to CN200 (DSC = 0.987) and MNI152 (DSC = 0.831), quantitatively demonstrating that the Kazakh female template provides a more geometrically appropriate reference space for this population than either alternative.

3.3 Cross-Template Registration Efficiency: Kazakh vs. MNI152 vs. CN200

The Kazakh template required significantly less deformation than both comparators; all pairwise contrasts reached significance after Bonferroni correction (Kazakh vs. CN200: $t(57) = -20.16$, $p = 1.3 \times 10^{-27}$, Cohen's $d = -1.46$; Kazakh vs. MNI152: $t(57) = -25.96$, $p = 2.9 \times 10^{-33}$, Cohen's $d = -4.49$).

Mean voxel-wise displacement magnitude was lowest when subjects were registered to the Kazakh template (2.630 ± 0.353 mm), intermediate for the CN200 template (3.246 ± 0.489 mm), and highest for the MNI152 template (6.191 ± 1.074 mm). In relative terms, registration to CN200 required 23.4% more deformation than registration to the Kazakh template, while registration to MNI152 required 135.4% more, a very large effect size for MNI152 (Cohen's $d = 4.49$) and moderate effect for CN200 (Cohen's $d = 1.46$). Paired contrasts confirmed that both the Kazakh and CN200 templates required significantly less deformation than MNI152 (Kazakh vs MNI152: $t(57) = -25.96$, $p < 0.001$; CN200 vs MNI152: $t(57) = 21.40$, $p < 0.001$). Full pairwise statistics are presented in Table 3.

The log-Jacobian analysis reveals a complementary picture in volumetric terms. The Kazakh template achieved the lowest systematic volumetric bias (mean log J = −0.032, equivalent to ~3.3% average volumetric adjustment), while CN200 showed an intermediate bias (mean log J = −0.060, equivalent to ~5.8%), whereas MNI152 showed the largest systematic volumetric bias (mean log J = −0.194, equivalent to ~17.6% systematic compression of subjects into the template space), consistent with MNI152 being derived from a predominantly larger volume Caucasian male weighted cohort with poor match to this population. MNI152 showed the greatest voxel-wise heterogeneity of log-Jacobian (SD of log J = 0.424, compared to 0.323 for both Kazakh and CN200), indicating that MNI152 fits Kazakh female brains in a much less uniform manner; some regions compress substantially while others expand, reflecting mismatched regional proportions. The spatial distribution of these deformation fields is visualised in Figure 2.

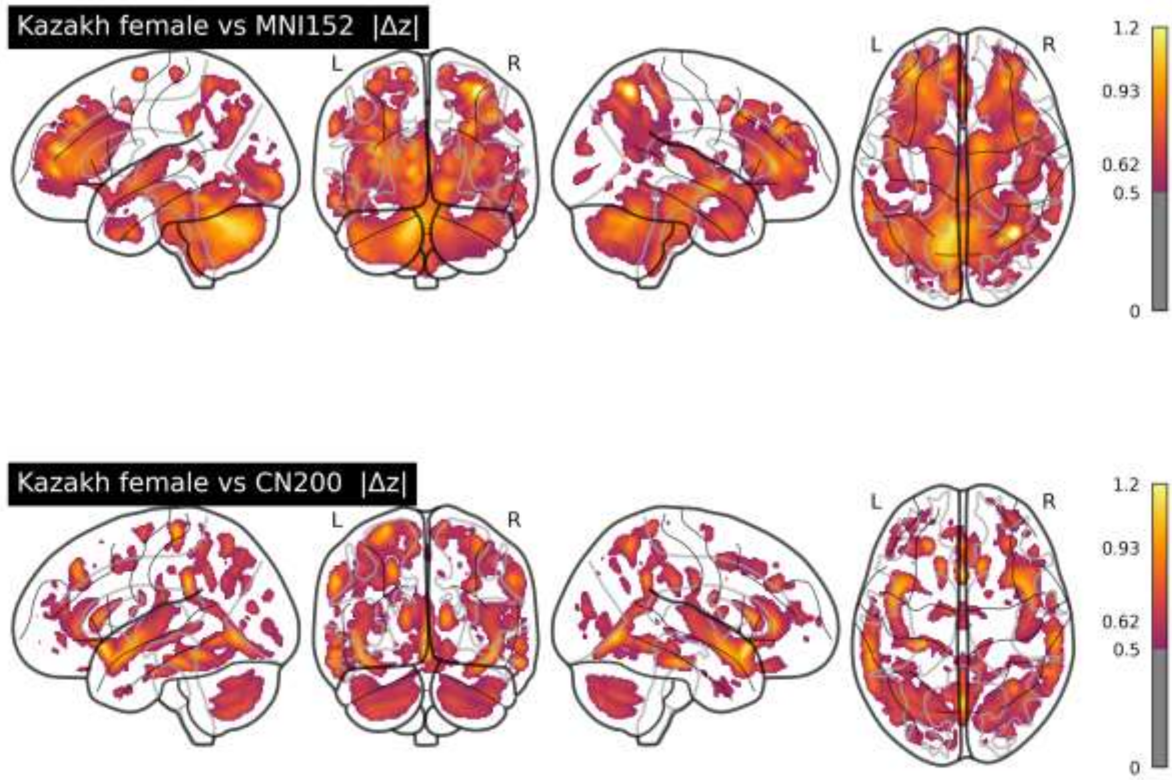

Figure 2. 3D spatial distribution of morphological divergence across standard templates. Glass-brain projections mapping the cross-template registration deformations required to align the Kazakh female template with the standard MNI152 (Western) and CN200 (East Asian) reference spaces. The visualizations highlight region-specific anatomical disparities, illustrating that alignment to the MNI152 template necessitates substantially larger spatial deformations (or local volumetric expansions/contractions) across the cortical surface compared to the biologically closer CN200 template.

In relative terms, registration to CN200 required 23.4% more deformation than registration to the Kazakh template, while registration to MNI152 required 135.4% more, representing a very large effect size for MNI152 (Cohen's $d = 4.49$) and a moderate effect for CN200 (Cohen's $d = 1.46$). Paired contrasts confirmed that both the Kazakh and CN200 templates provided a significantly better anatomical fit than MNI152. The statistical significance of these cross-template comparisons is summarized in **Table 2**.

Table 2. Global deformation field properties and baseline cross-template registration metrics (n = 58).

template	n	mean_u	sd_u	mean_logJ	sd_logJ	DSC	NCC	delta_u_pct
CN200	58	3.245523099	0.488717294	-0.0598107532	0.3621392194	0.987309233	0.9779312549	23.4
Kazakh	58	2.629739067	0.3532045968	-0.03234519911	0.3230797325	0.9938789513	0.9877645312	0
MNI152	58	6.191381405	1.074448865	-0.1937163086	0.4247724789	0.8311133826	0.6172935017	135.4

|u| = voxel-wise magnitude of the deformation field (mm), averaged within the brain mask. log J = log-Jacobian determinant of the deformation field; a mean near zero indicates minimal systematic volumetric adjustment, larger SD indicates more heterogeneous local volumetric adjustment. Δ|u| reports the relative increase in mean deformation magnitude compared with the Kazakh template. Cohen's d was computed with the pooled SD. All templates were resampled to a common 1 mm isotropic resolution prior to registration.

Table 3. Pairwise post-hoc t-test contrasts verifying the significance of registration efficiency gaps

pair	metric	t	p	sig	cohen_d
Kazakh vs MNI152	mean_u	-25.95943246	2.90E-33	***	-4.492351092
Kazakh vs CN200	mean_u	-20.16441554	1.28E-27	***	-1.456831083
MNI152 vs CN200	mean_u	21.39919065	6.37E-29	***	3.560274193
Kazakh vs MNI152	mean_logJ	6.982256411	3.41E-09	***	1.336401127
Kazakh vs CN200	mean_logJ	21.17439671	1.09E-28	***	1.087760302
MNI152 vs CN200	mean_logJ	-5.792899407	3.13E-07	***	-1.108136478

*t = paired t-statistic; p = two-tailed p-value after Bonferroni correction (family-wise $\alpha = 0.05$ across three pairwise contrasts); sig = significance level (*** $p < 0.001$); Cohen's d = standardised effect size computed with pooled SD. Positive d indicates greater deformation for the first-named template; negative d indicates greater deformation for the second-named template.*

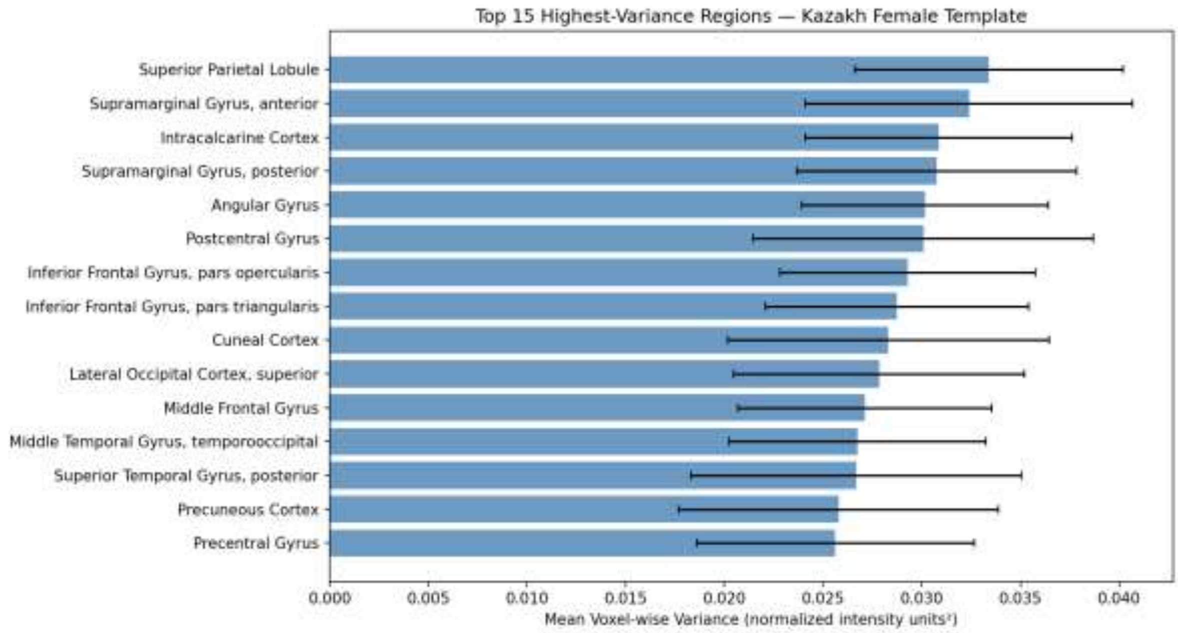

Figure 3. *Horizontal bar chart showing mean voxel-wise variance (± SD, normalized intensity units²) per region, ranked in descending order, computed from the 58 warped subject volumes using the Harvard-Oxford Cortical parcellation warped into native Kazakh template space. Error bars represent one standard deviation across in-region voxels. Regions are sorted by mean variance; the five highest-variance regions are concentrated in posterior parietal and occipital cortex, consistent with the voxel-wise divergence pattern observed against MNI152 (Section 3.4).*

3.4 Comparison with MNI152 Standard Space

The macroscopic structural alignment between the pooled Kazakh female template and the MNI152 (ICBM, 2009c) standard was strong. Non-linear SyN registration yielded a physical overlap of 3,180,888 brain voxels. Voxel-wise intensity comparison across this overlapping region returned a Pearson correlation of $r = 0.718$ with a mean absolute error of MAE = 0.207. Visual and quantitative comparisons are shown in Figure 4. The coefficient of determination $r^2 = 0.515$ indicates that 51.5% of voxel-wise variance is shared between the Kazakh female template and MNI152, leaving approximately 48.5% unexplained. To contextualize this divergence, the same voxel-wise intensity comparison was repeated between the Kazakh female template and the CN200 template. This analysis yielded $r = 0.988$, $r^2 = 0.976$, MAE = 0.033 across 3,440,910 overlapping voxels and a coefficient of determination 89.4% higher than that observed against MNI152 ($r^2 = 0.515$)(see Table 4 for full cross-template comparison). The near unity correspondence with CN200 confirms that the unexplained variance against MNI152 reflects genuine population level morphological divergence rather than a registration or preprocessing artifact, and establishes that Kazakh female neuroanatomy is substantially closer to the East Asian CN200 reference than to the Caucasian MNI152 standard. The residual variance suggests morphological divergence that may exceed what is attributable to registration error alone, though a formal decomposition was not performed.

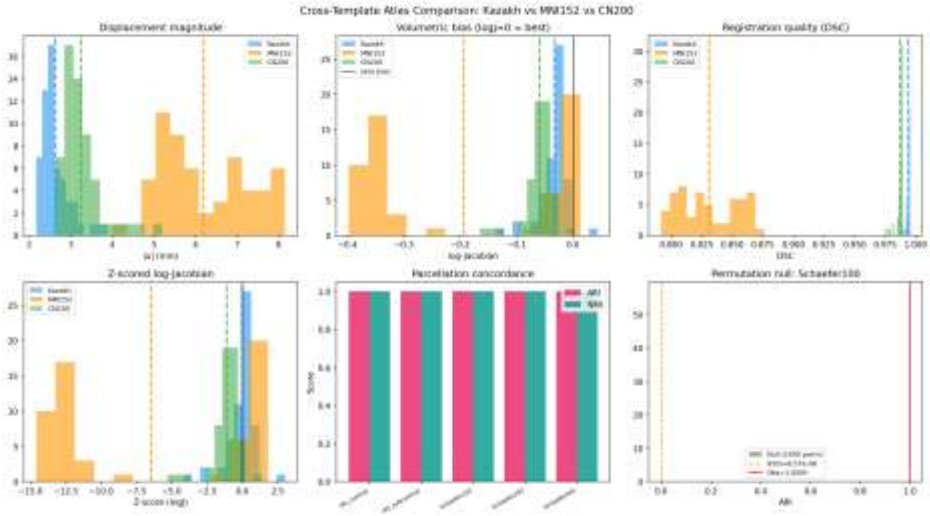

Figure 4. Structural comparison and voxel-wise intensity correlation between the Kazakh female template and the MNI152 standard. (A) Visual overlay of the anatomical boundaries highlights systematic structural displacements, particularly prominent across the cortical mantle, frontal regions, and ventricular margins. (B) Joint-intensity scatter plot computed across the 3,180,888 overlapping brain voxels.

Table 4. Voxel-wise cross-template intensity correlations and continuous error profiles

comparison	n_voxels	r	r2	MAE
Kazakh vs MNI152	3180888	0.7177533142	0.51516982	0.2068446051
Kazakh vs CN200	3440910	0.9878019147	0.9757526226	0.03296416869
MNI152 vs CN200	4629572	0.7467867936	0.557690515	0.1706297991

r = Pearson correlation coefficient computed voxel-wise across the overlapping brain mask between normalized [0, 1] intensity images; r^2 = coefficient of determination, representing the proportion of voxel-wise intensity variance shared between the two templates; MAE = mean absolute error on the same [0, 1] intensity scale; n voxels = number of overlapping brain-mask voxels contributing to each comparison. All templates were resampled to a common 1 mm isotropic resolution and intensity-normalized to [0, 1] via percentile-based clipping (1st–99th percentile over non-zero voxels) prior to comparison. MNI152 self-registration under the same SyN pipeline returned r^2 = 1.000, confirming that residual variance in the Kazakh vs. MNI152 comparison reflects anatomical divergence rather than registration or preprocessing artifact.

Voxel-wise variance maps localized the greatest anatomical divergence to the cortical mantle, particularly the superior frontal gyrus, the precuneus, the cuneus, and the lingual gyrus, and to the boundaries of the lateral ventricular system. By contrast, deep gray matter nuclei (thalamus, putamen, caudate) and the brainstem showed minimal divergence, consistent with greater evolutionary conservation of subcortical morphology. The spatial specificity of inter individual variability to the posterior parietal and occipital cortex is further illustrated by the regional breakdown in Figure 3.

3.5 Topological Concordance with Global Parcellation Atlases

When the Kazakh female template was compared with four widely used MNI-space parcellations, concordance was consistently high, demonstrating strong topological correspondence across all atlas types (Table 5). The Harvard-Oxford Subcortical atlas achieved substantial agreement (ARI = 0.347; NMI = 0.435), reflecting the cross-population stability of subcortical boundaries. Cortical concordance was also strong: Harvard-Oxford Cortical returned ARI = 0.319 and NMI = 0.635, while the three Schaefer 2018 parcellations yielded ARI values between 0.345 and 0.360 at NMI ranging from 0.728 to 0.771.

The modest decline in ARI with increasing Schaefer granularity (0.360 → 0.352 → 0.345 for 100 → 200 → 400 parcels) is diagnostically informative. The gradual, rather than sharp, reduction indicates that the Kazakh template retains meaningful topological correspondence even at finer parcellation scales, with high-ARI agreement reflecting genuine shared sulcal and gyral topology between the Kazakh female brain and Caucasian-derived parcellations. This information theoretic signature provides resolution independent, quantitative evidence of anatomical correspondence, while the high NMI values (0.728–0.771 for Schaefer atlases) further confirm the informativeness of the Kazakh template as a reference frame.To confirm these values reflect genuine anatomical signal rather than chance level overlap, 1,000-permutation null distributions were constructed at each granularity level by randomly permuting Schaefer labels while preserving label count distributions. The null distributions were tightly centered on zero (mean ± SD: $-7.1\times10^{-8} \pm 5.0\times10^{-6}$, $1.9\times10^{-7} \pm 3.0\times10^{-6}$, and $-1.4\times10^{-8} \pm 3.0\times10^{-6}$ for 100, 200, and 400 parcels, respectively), with 95th percentile values of 8×10^{-6}, 5×10^{-6}, and 4×10^{-6}. Observed ARI values (0.360, 0.352, and 0.345) exceeded the 95th percentile of the corresponding null distributions at all three granularities (permutation $p < 0.001$ in all cases), confirming statistically significant and strong anatomical correspondence between the Kazakh female template and Caucasian-derived Schaefer parcellations.

To assess whether observed ARI values exceeded chance, a permutation null distribution was constructed for each Schaefer granularity (100, 200, and 400 parcels). Schaefer parcel labels in the warped Kazakh template space were randomly permuted 1,000 times per granularity, preserving label-count distributions while destroying spatial correspondence. ARI was recomputed for each permutation, and the observed ARI was ranked against this null distribution; statistical significance was declared when the observed ARI exceeded the 95th percentile (one-tailed, $\alpha = 0.05$). **Figure 5** displays the permutation null distributions for each Schaefer granularity alongside the observed ARI values.

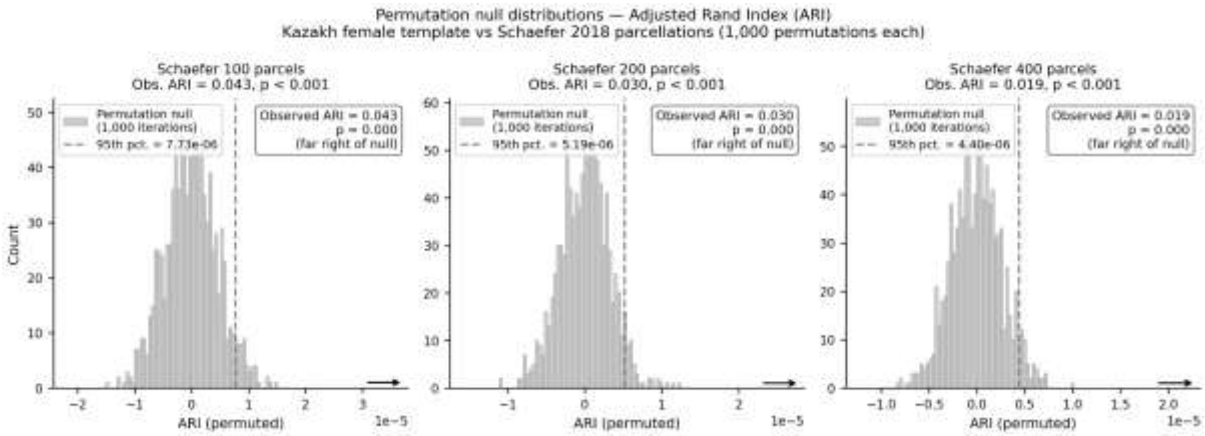

Figure 5. Permutation null distributions for each Schaefer granularity. ***Permutation null distributions for the Adjusted Rand Index (ARI) comparing the Kazakh female template parcellation against the Schaefer 2018 atlas at three granularities (100, 200, and 400 parcels). Each null distribution was constructed from 1,000 random label permutations: the spatial arrangement of labels was destroyed while preserving label-count distributions. Grey histograms: null distributions (all concentrated at ARI ≈ 0). Dashed vertical line: 95th percentile of null. Observed ARI values (annotated boxes) exceed the null ceiling by three to four orders of magnitude (p < 0.001 at all granularities, permutation test).***

Table 5. Topological cross-population atlas concordance metrics integrated with permutation validation targets.

atlas	n_voxels	ARI	NMI	Observed ARI	null 95	Perm pval

HO_cortical	377835	0.3191	0.6351	-	-	-
HO_subcortical	943293	0.3469	0.4352	-	-	-
Schaefer100	388450	0.3598	0.7278	0. 3597740803	1.58E-05	<0.0001
Schaefer200	388450	0.3522	0.753	0. 352159226	1.09E-05	<0.0001
Schaefer400	388450	0.3451	0.7709	0. 3450955794	8.23E-06	<0.0001

ARI = Adjusted Rand Index; NMI = Normalized Mutual Information; n voxels = number of overlapping voxels between the warped parcellation and the Kazakh template brain mask. ARI quantifies parcellation similarity above chance (ARI = 1: identical partitioning; ARI ≈ 0: chance-level agreement). NMI ranges from 0 to 1 and is insensitive to the absolute number of parcels, enabling comparison across atlases of differing granularity. Permutation p-values (perm p) were derived from 1,000-permutation null distributions constructed by randomly permuting parcel labels while preserving label-count distributions; all observed ARI values exceeded the 95th percentile of the corresponding null distribution ($p < 0.001$). Null distributions were tightly centered on zero (mean < 10^{-7}, SD < 10^{-5} at all granularities). Permutation testing was applied to Schaefer 2018 parcellations only; Harvard-Oxford atlases were not subjected to permutation validation. HO = Harvard-Oxford; ARI and NMI are not applicable to continuous intensity comparisons.

3.6 Voxel-wise Variance Analysis

Voxel-wise variance maps across the 58 contributing subjects were computed to characterize the spatial distribution of inter-individual anatomical variability (Figure 5). Variance was greatest in the cortical mantle, particularly in gyral crowns of the superior frontal, precentral, and supramarginal gyri, and along ventricular boundaries. Minimal variance was observed in deep white matter, the corpus callosum, and brainstem structures. This spatial pattern is congruent with the voxel-level divergence observed against MNI152 (Section 3.4) and supports the interpretation that population specific anatomical variability is concentrated in the same structures where Kazakh and Caucasian references differ most.

Quantitative extraction of peak variance regions identified the following five anatomical locations as showing the greatest inter-subject variability (mean voxel-wise variance ± SD, normalized intensity units^2): Superior Parietal Lobule (0.0334 ± 0.0068), Supramarginal Gyrus anterior division (0.0324 ± 0.0083), Intracalcarine Cortex (0.0309 ± 0.0068), Supramarginal Gyrus posterior division (0.0308 ± 0.0071), and Angular Gyrus (0.0302 ± 0.0062). The lowest variance was observed in medial structures, including Subcallosal Cortex (0.0140 ± 0.0048), Parahippocampal Gyrus anterior division (0.0150 ± 0.0042), and Insular Cortex (0.0152 ± 0.0032), confirming spatial specificity of inter-individual variability to posterior parietal and occipital cortex.

4 Discussion

This study presents the first female-specific structural MRI template for the Kazakh population. Three principal outcomes emerge from this framework. First, construction of the iterative unbiased template converged with high internal fidelity across the 58 subject cohort (mean LOO-CV DSC = 0.987 ± 0.004, mean NCC = 0.874 ± 0.071), establishing a geometrically central reference frame for Kazakh female neuroanatomy. Second, despite strong global correlation with MNI152 (r = 0.718), the coefficient of determination (r^2 = 0.515) reveals that 48.5% of voxel-wise structural variance is unshared with MNI152, while topological concordance with Caucasian-derived anatomical and functional parcellations was systematically constrained (cortical ARI ranges from 0.319 to 0.360). Third, direct cross-template registration established a clear ranking: the Kazakh template provides the best anatomical match; CN200 is a substantially closer match than MNI152 (23.4% vs. 135.4% additional deformation); and the Kazakh template shows the lowest systematic volumetric bias of the three.

4.1 Global Alignment Masks Local Divergence

Perhaps the most clinically consequential observation of this work is the dissociation between global and local concordance metrics. A voxel-wise Pearson correlation of r = 0.718 with MNI152 might conventionally be read as satisfactory anatomical alignment; however, the coefficient of determination $r^2 = 0.515$ reveals that nearly half of voxel-wise structural variance is unshared with MNI152, while cortical parcellation concordance (ARI = 0.319–0.360) though statistically significant and far above chance (permutation $p < 0.001$ at all granularities) ,which indicates that meaningful gyral and sulcal boundary displacement exists relative to Caucasian-derived references. These moderate ARI values should not be interpreted as indicating either full concordance or complete divergence: they reflect a population whose macroscopic topology is recognizably related to Western templates but whose regional boundaries are systematically shifted in ways that carry direct consequences for automated morphometry and parcellation-based analyses. In other words, although the Kazakh template occupies the same standard coordinate system as MNI152, the gyral and sulcal landmarks that define clinically meaningful regions do not coincide with the MNI-based parcel boundaries. This pattern closely parallels findings from the studies of Chinese [4] and Indian [16] template initiatives, which similarly report high global correlation with MNI152, accompanied by measurable cortical-boundary displacement.

The modest decline of ARI with increasing Schaefer granularity (0.360 → 0.352 → 0.345 for 100 → 200 → 400 parcels) is diagnostically important. The high ARI values at all granularities confirm that the topological correspondence between the Kazakh template and Caucasian-derived Schaefer parcellations is genuine. The gradual, rather than sharp, decline indicates that this correspondence is maintained even at fine scales, with fine granularity retaining meaningful correspondence, indicating that the Kazakh female brain shares a high degree of gyral and sulcal topology with Caucasian references. This mathematical signature supports the utility of the Kazakh template as a compatible reference frame for existing MNI-space parcellations, while still justifying its value for the residual 48.5% unexplained voxel-wise variance and the superior deformation field fit relative to both MNI152 and CN200.

4.2 Mitigating Unisex and Population Bias in Neuroimaging

The use of unisex, Western-derived templates in studies of non-Western populations introduces well documented biases into both volumetric and surface-based morphometry [13,17,24,37]. Male and female brains differ not only in mean global volume but in the pattern and magnitude of regional variability and in their lifespan trajectories [7,8]. Unisex atlases average across these differences, attenuating sensitivity to sex-specific anatomical features and reducing statistical power to detect pathology with sex-specific expression, most notably Alzheimer's disease, where female patients show accelerated posterior cingulate and precuneal atrophy relative to male patients matched for clinical severity [14].

A key finding of the present study is that the East Asian CN200 template performs substantially better than the Caucasian MNI152 template for Kazakh female subjects (23.4% vs. 135.4% greater deformation than the Kazakh template; MNI152 Cohen's $d = 4.49$ vs. CN200 Cohen's $d = 1.46$, both $p < 0.001$). This neuroimaging result has direct methodological implications: the widespread practice of deploying MNI152 as the default reference for populations lacking dedicated templates introduces substantially greater registration error for this population than the East Asian CN200, and CN200 represents the less biased global default in the absence of a Kazakh specific reference.

One possible, non-exclusive explanation for this pattern is population genetic: published genome wide studies report that Kazakh individuals carry substantial East Asian autosomal ancestry alongside West Eurasian components [19,20,38], and the closer match of CN200 to Kazakh neuroanatomy may reflect shared East Asian cranial and cortical morphology. However, no genetic data were collected from participants in this study, and this interpretation rests entirely on external literature. Alternative explanations that cannot be excluded include: systematic differences in nutritional environment and socioeconomic conditions between the Kazakh cohort and the MNI152 construction sample; cohort composition differences (e.g., age range, sex ratio, or urban vs. rural sampling); or the larger brain volumes and Caucasian male bias of the MNI152 reference cohort. The neuroanatomical data are consistent with, but do not constitute direct evidence for any of these explanations.

Importantly, the Kazakh template outperforms both MNI152 and CN200 in total deformation and volumetric bias, confirming that the population has a distinct neuroanatomical profile that is closer to East Asian than to Caucasian global references

4.3 Clinical Implications for Dementia and Alzheimer's Disease

The template presented here is designed to serve as a biologically matched reference for clinical and research neuroimaging in Central Asia, with three specific methodological applications. First, in AD screening, the population-specific template is hypothesized to enable detection of pathological atrophy against a sex and ethnicity matched baseline, which is hypothesized to reduce false positive rates arising when healthy Kazakh cortical morphology is interpreted against Caucasian normative ranges, though this benefit remains to be formally quantified in a prospective diagnostic validation study. Second, in VBM, registration to the Kazakh female template is hypothesized to improve the statistical sensitivity of group level analyses in the local population, since residual registration error is absorbed into the noise floor of any VBM study. Third, in stereotactic surgical planning and in automated segmentation pipelines (including deep-learning segmentation tools, which inherit the biases of their training atlases [24,26], the template is hypothesized to provide a more anatomically appropriate landmark framework than current global standards.

The clinical benefits described above constitute testable hypotheses rather than established findings of the present study. A prospective validation study comparing automated atrophy detection performance with and without the Kazakh template in a confirmed early stage AD cohort is a logical next step and is currently in planning.

4.4 Limitations and Future Directions

Several limitations should be acknowledged. First, the sample size (n = 58) is modest, though cohort homogeneity and image quality are of greater consequence than raw size for population-specific template construction [4,31], and our sample exceeds several published precedents. Second, four participants were excluded due to off protocol acquisitions identified retrospectively; the absence of a formal real time QC protocol and radiologist oversight during acquisition precluded prospective detection or rescanning. Future collections will implement a session level QC checklist with radiologist signoff. Third, the native template was acquired at anisotropic resolution ($0.89 \times 0.89 \times 1.5$ mm^3), with through-plane resolution ~40% coarser than in plane. This disproportionately affects MTL structures critical to early Alzheimer's detection (hippocampus, entorhinal cortex, parahippocampal gyrus, amygdala), with estimated parcellation boundary displacement of 1–2 voxels (1.5–3.0 mm) in the through plane direction [31]. Resampling to 1 mm isotropic prior to cross-template comparison partially mitigates this; the coreleased MNI-space 1 mm isotropic variant is recommended over the native template for MTL parcellation pending isotropic reacquisition. Fourth, recruitment from a single urban center (Astana) limits generalizability to rural and geographically dispersed Kazakhstani populations. Fifth, the present template covers only females; a complementary male Kazakh template is in preparation and will permit direct evaluation of sex effects within the same population. Sixth, brain extraction was performed with FSL BET at a starting fractional intensity threshold of f = 0.5, selected empirically to preserve inferior frontal and temporal cortex. Six of 58 subjects (10.3%) required posthoc reprocessing with adjusted thresholds (f = 0.46–0.70) to resolve residual extracerebral tissue inclusion identified during manual quality control; one subject additionally required FSL robustFOV neck cropping prior to re-extraction. Following these remediations, all 58 subjects met quantitative acceptance thresholds (DSC > 0.97, NCC > 0.60) on LOO-CV. Brain extraction quality is reported as aggregate LOO-CV DSC; false positive and false negative voxel rates were not computed separately, which limits granular mask error characterisation. Future iterations will evaluate deep-learning based extraction tools such as HD-BET or SynthStrip, which have demonstrated improved zero-shot consistency on anisotropic acquisitions. Seventh, imaging at 1.5 T limits gray to white contrast relative to 3 T. Finally, the cross sectional design cannot distinguish cohort from aging effects; longitudinal followup is planned.

Future work will pursue: (i) a parallel male template and unified Kazakh age-and-sex atlas; (ii) multi-site validation across Almaty, Shymkent, and rural oblasts; and (iii) clinical benchmarking in a prospective AD-screening cohort to quantify the diagnostic benefit of population-matched references.

5 Conclusion

We have constructed and validated the first female-specific MRI brain template for the Kazakh population, addressing a gap in Global neuroimaging standards. Our template achieves high internal registration fidelity and aligns successfully with MNI152 space, yet shows systematically low topological concordance with Western-derived cortical parcellations quantified by $r^2 = 0.515$ and ARI of 0.319–0.360, providing rigorous quantitative evidence that Kazakh female neuroanatomy cannot be adequately represented by MNI152 despite strong parcellation concordance with Caucasian derived atlases. Cross-template comparison further establishes that a Caucasian reference (MNI152) performs substantially inferior to an East Asian reference (CN200) for this population in terms of deformation magnitude, a finding consistent with Kazakh population genetic admixture and not previously demonstrated neuroanatomically. By providing a biologically matched, population-specific baseline, this template offers a methodologically grounded reference for future clinical and research morphometry in Central Asia. Its diagnostic utility for early neurodegenerative disease detection in particular Alzheimer's disease screening remains to be established through prospective clinical benchmarking, which is currently in planning.

6 Abbreviations

AD - Alzheimer's disease; ANTs - Advanced Normalization Tools; ARI - Adjusted Rand Index; BET - Brain Extraction Tool; DSC - Dice Similarity Coefficient; FOV - Field of View; FSL - FMRIB Software Library; GM - Gray Matter; H-O - Harvard-Oxford Atlas; MAE - Mean Absolute Error; MoCA - Montreal Cognitive Assessment; MRI - Magnetic Resonance Imaging; NCC - Normalized Cross-Correlation; NIfTI - Neuroimaging Informatics Technology Initiative; NMI - Normalized Mutual Information; RAS - Right-Anterior-Superior; RRID - Research Resource Identifier; SES - Socioeconomic Status; SyN - Symmetric Normalization; TE - Echo Time; TIV - Total Intracranial Volume; TR - Repetition Time; VBM - Voxel-Based Morphometry; WM - White Matter.

7 Conflict of Interest

The authors declare that the research was conducted in the absence of any commercial or financial relationships that could be construed as a potential conflict of interest.

8 Author Contributions

MK - Writing (Original Draft), Methodology, Formal Analysis. AT - Writing (Original Draft), Software, Formal Analysis. AiB - Writing (Original Draft), Methodology, Investigation, Data Curation, Project Administration. NZ - Writing (Original Draft), Investigation, Visualization. EA - Writing (Original Draft), Investigation, Formal Analysis. AlB - Writing (Original Draft), Investigation, Data Curation. JA - Writing (Review & Editing), Methodology, Validation, SHA - Writing (Review & Editing), Methodology, Validation. SB - Writing (Review & Editing), Conceptualization, Funding Acquisition, Resources, Supervision, Project Administration. All authors have read and approved the final manuscript.

9 Funding

This study was funded by the Ministry of Science and Higher Education of the Republic of Kazakhstan (Grant No. AP26199361, "Investigating the Relationship Between Sleep Quality and Brain Imaging Biomarkers") and by the Nazarbayev University Faculty Development Competitive Research Grant Program 2024–2026 (Grant No. SOM2024008, "Construction of the Kazakh Brain Atlas and its role in the improvement of AI-based diagnostics of Dementia and Alzheimer's disease"). The sponsors had no role in study design; in the collection, analysis, or interpretation of data; in the writing of the report; or in the decision to submit the paper for publication.

10 Acknowledgments

The authors thank the participants of the Kazakh Brain Atlas cohort for their time and engagement, the radiology and MRI technical staff of the Mother and Child Center, University Medical Center (Astana), for scanning support, and the Research Ethics Committee of Nazarbayev University for regulatory oversight. Computing resources were provided by the School of Medicine, Nazarbayev University.

11 Data Availability Statement

The pooled Kazakh female template, together with all processing notebooks and container specifications required to reproduce the pipeline, will be released upon publication via the OSF repository at [INSERT OSF DOI] under a Creative Commons Attribution 4.0 license. Deidentified individual T1 volumes underlying the template are available from the corresponding author upon reasonable request and following completion of a data use agreement, consistent with the conditions of participant consent. Deidentified individual T1 volumes underlying the templates are available from the corresponding author upon reasonable request and following completion of a data use agreement, consistent with the conditions of participant consent.

12 References

1. Mazziotta J, Toga A, Evans A, Fox P, Lancaster J, Zilles K, et al. A probabilistic atlas and reference system for the human brain: International Consortium for Brain Mapping (ICBM). Kötter R, editor. Philos Trans R Soc Lond B Biol Sci. 2001 Aug 29;356(1412):1293–322. doi:10.1098/rstb.2001.0915

2. Giff A, Noren G, Magnotti J, Lopes AC, Batistuzzo MC, Hoexter M, et al. Spatial normalization discrepancies between native and MNI152 brain template scans in gamma ventral capsulotomy patients. Psychiatry Res Neuroimaging. 2023 Mar;329:111595. doi:10.1016/j.pscychresns.2023.111595

3. Tang Y, Hojatkashani C, Dinov ID, Sun B, Fan L, Lin X, et al. The construction of a Chinese MRI brain atlas: A morphometric comparison study between Chinese and Caucasian cohorts. NeuroImage. 2010 May;51(1):33–41. doi:10.1016/j.neuroimage.2010.01.111

4. Yang G, Zhou S, Bozek J, Dong HM, Han M, Zuo XN, et al. Sample sizes and population differences in brain template construction. NeuroImage. 2020 Feb;206:116318. doi:10.1016/j.neuroimage.2019.116318

5. Liang P, Shi L, Chen N, Luo Y, Wang X, Liu K, et al. Construction of brain atlases based on a multi-center MRI dataset of 2020 Chinese adults. Sci Rep. 2015 Dec 18;5(1):18216. doi:10.1038/srep18216

6. Valter Y, Huang Y, Khadka N, Bikson M, Datta A. Morphological bias of the MNI152 brain [Internet]. Neuroscience; 2026 [cited 2026 May 29]. Available from: http://biorxiv.org/lookup/doi/10.64898/2026.01.24.701532 doi:10.64898/2026.01.24.701532

7. Ruigrok ANV, Salimi-Khorshidi G, Lai MC, Baron-Cohen S, Lombardo MV, Tait RJ, et al. A meta-analysis of sex differences in human brain structure. Neurosci Biobehav Rev. 2014 Feb;39:34–50. doi:10.1016/j.neubiorev.2013.12.004

8. Lotze M, Domin M, Gerlach FH, Gaser C, Lueders E, Schmidt CO, et al. Novel findings from 2,838 Adult Brains on Sex Differences in Gray Matter Brain Volume. Sci Rep. 2019 Feb 8;9(1):1671. doi:10.1038/s41598-018-38239-2

9. Salminen LE, Tubi MA, Bright J, Thomopoulos SI, Wieand A, Thompson PM. Sex is a defining feature of neuroimaging phenotypes in major brain disorders. Hum Brain Mapp. 2022 Jan;43(1):500–42. doi:10.1002/hbm.25438

10. Ingalhalikar M, Smith A, Parker D, Satterthwaite TD, Elliott MA, Ruparel K, et al. Sex differences in the structural connectome of the human brain. Proc Natl Acad Sci. 2014 Jan 14;111(2):823–8. doi:10.1073/pnas.1316909110

11. Choi YY, Lee JJ, Choi KY, Choi US, Seo EH, Choo IH, et al. Multi-Racial Normative Data for Lobar and Subcortical Brain Volumes in Old Age: Korean and Caucasian Norms May Be Incompatible With Each Other†. Front Aging Neurosci. 2021 Aug 3;13:675016. doi:10.3389/fnagi.2021.675016

12. Austin TR, Nasrallah IM, Erus G, Desiderio LM, Chen LY, Greenland P, et al. Association of Brain Volumes and White Matter Injury With Race, Ethnicity, and Cardiovascular Risk Factors: The Multi-Ethnic Study of Atherosclerosis. J Am Heart Assoc. 2022 Apr 5;11(7):e023159. doi:10.1161/JAHA.121.023159

13. Atilano-Barbosa D, Barrios FA. Brain morphological variability between whites and African Americans: the importance of racial identity in brain imaging research. Front Integr Neurosci. 2023 Dec 21;17:1027382. doi:10.3389/fnint.2023.1027382

14. Nebel RA, Aggarwal NT, Barnes LL, Gallagher A, Goldstein JM, Kantarci K, et al. Understanding the impact of sex and gender in Alzheimer's disease: A call to action. Alzheimers Dement. 2018 Sep;14(9):1171–83. doi:10.1016/j.jalz.2018.04.008

15. Prince M, Ali GC, Guerchet M, Prina AM, Albanese E, Wu YT. Recent global trends in the prevalence and incidence of dementia, and survival with dementia. Alzheimers Res Ther. 2016 Dec;8(1):23. doi:10.1186/s13195-016-0188-8

16. Bhalerao GV, Parlikar R, Agrawal R, Shivakumar V, Kalmady SV, Rao NP, et al. Construction of population-specific Indian MRI brain template: Morphometric comparison with Chinese and Caucasian templates. Asian J Psychiatry. 2018 Jun;35:93–100. doi:10.1016/j.ajp.2018.05.014

17. Choi YY, Lee JJ, Choi KY, Seo EH, Choo IH, Kim H, et al. The Aging Slopes of Brain Structures Vary by Ethnicity and Sex: Evidence From a Large Magnetic Resonance Imaging Dataset From a Single Scanner of Cognitively Healthy Elderly People in Korea. Front Aging Neurosci. 2020 Aug 12;12:233. doi:10.3389/fnagi.2020.00233

18. United Nations Convention to Combat Desertification. (2023). Regional factsheet: Central Asia. UNCCD Secretariat. https://www.unccd.int

19. Jeong C, Balanovsky O, Lukianova E, Kahbatkyzy N, Flegontov P, Zaporozhchenko V, et al. The genetic history of admixture across inner Eurasia. Nat Ecol Evol. 2019 Apr 29;3(6):966–76. doi:10.1038/s41559-019-0878-2

20. Yunusbayev B, Metspalu M, Jarve M, Kutuev I, Rootsi S, Metspalu E, et al. The Caucasus as an Asymmetric Semipermeable Barrier to Ancient Human Migrations. Mol Biol Evol. 2012 Jan 1;29(1):359–65. doi:10.1093/molbev/msr221

21. Lei C, Liu J, Zhang R, Pan Y, Lu Y, Gao Y, et al. Ancestral Origins and Admixture History of Kazakhs. Ávila-Arcos MC, editor. Mol Biol Evol. 2024 Jul 3;41(7):msae144. doi:10.1093/molbev/msae144

22. Yang MH, Kim EH, Choi ES, Ko H. Comparison of Normative Percentiles of Brain Volume Obtained from NeuroQuant® vs. DeepBrain® in the Korean Population: Correlation with Cranial Shape. J Korean Soc Radiol. 2023;84(5):1080. doi:10.3348/jksr.2023.0006

23. NeuroQuant Normative Database: Advancing Age- and Sex-Specific Brain Volumetry - Cortechs.ai [Internet]. 2026 Feb 11 [cited 2026 May 29]. Available from: https://www.cortechs.ai/neuroquant-normative-database-advancing-age%E2%80%91-and-sex%E2%80%91specific-brain-volumetry/

24. Danaee G, Niethammer M, Rushmore J, Bouix S. Investigating Demographic Bias in Brain MRI Segmentation: A Comparative Study of Deep-Learning and Non-Deep-Learning Methods. Mach Learn Biomed Imaging. 2025 Dec 30;3(Special on FAIMI):792–808. doi:10.59275/j.melba.2025-d1g3

25. Seyyed-Kalantari L, Zhang H, McDermott MBA, Chen IY, Ghassemi M. Underdiagnosis bias of artificial intelligence algorithms applied to chest radiographs in under-served patient populations. Nat Med. 2021 Dec;27(12):2176–82. doi:10.1038/s41591-021-01595-0

26. Sabuncu MR, Wang AQ, Nguyen M. Ethical Use of Artificial Intelligence in Medical Diagnostics Demands a Focus on Accuracy, Not Fairness. NEJM AI. 2025 Jan;2(1). doi:10.1056/AIp2400672

27. Koçak B, Ponsiglione A, Stanzione A, Bluethgen C, Santinha J, Ugga L, et al. Bias in artificial intelligence for medical imaging: fundamentals, detection, avoidance, mitigation, challenges, ethics, and prospects. Diagn Interv Radiol. 2024 Jul 2. doi:10.4274/dir.2024.242854

28. Jafari B, Memar M. Exploring mesoscale brain connectivity variations and developing sex-specific tractography templates. NeuroImage. 2025 Nov;322:121545. doi:10.1016/j.neuroimage.2025.121545

29. Shima K, Matsunari I, Samuraki M, Chen WP, Yanase D, Noguchi-Shinohara M, et al. Posterior cingulate atrophy and metabolic decline in early stage Alzheimer's disease. Neurobiol Aging. 2012 Sep;33(9):2006–17. doi:10.1016/j.neurobiolaging.2011.07.009

30. Avants BB, Tustison NJ, Song G, Cook PA, Klein A, Gee JC. A reproducible evaluation of ANTs similarity metric performance in brain image registration. NeuroImage. 2011 Feb;54(3):2033–44. doi:10.1016/j.neuroimage.2010.09.025

31. Fillmore PT, Phillips-Meek MC, Richards JE. Age-specific MRI brain and head templates for healthy adults from 20 through 89 years of age. Front Aging Neurosci. 2015 Apr 8;7. doi:10.3389/fnagi.2015.00044

32. Wang S, Jiang Y, Yang A, Meng F, Zhang J. The Expanding Burden of Neurodegenerative Diseases: An Unmet Medical and Social Need. Aging Dis. 2024;0. doi:10.14336/AD.2024.1071

33. Nasreddine ZS, Phillips NA, Bédirian V, Charbonneau S, Whitehead V, Collin I, et al. The Montreal Cognitive Assessment, MoCA: A Brief Screening Tool For Mild Cognitive Impairment. J Am Geriatr Soc. 2005 Apr;53(4):695–9. doi:10.1111/j.1532-5415.2005.53221.x

34. Tustison NJ, Avants BB, Cook PA, Yuanjie Zheng, Egan A, Yushkevich PA, et al. N4ITK: Improved N3 Bias Correction. IEEE Trans Med Imaging. 2010 Jun;29(6):1310–20. doi:10.1109/TMI.2010.2046908

35. Fonov V, Evans AC, Botteron K, Almli CR, McKinstry RC, Collins DL. Unbiased average age-appropriate atlases for pediatric studies. NeuroImage. 2011 Jan;54(1):313–27. doi:10.1016/j.neuroimage.2010.07.033

36. Vinh NX, Vinh NX, Epps J, Epps J, Bailey J. Information Theoretic Measures for Clusterings Comparison: Variants, Properties, Normalization and Correction for Chance.

37. Choi YY, Lee JJ, Te Nijenhuis J, Choi KY, Park J, Ok J, et al. Multi-Ethnic Norms for Volumes of Subcortical and Lobar Brain Structures Measured by Neuro I: Ethnicity May Improve the Diagnosis of Alzheimer's Disease. J Alzheimer's Dis. 2024 Apr 30;99(1):223–40. doi:10.3233/JAD-231182

38. Metspalu M, Romero IG, Yunusbayev B, Chaubey G, Mallick CB, Hudjashov G, et al. Shared and Unique Components of Human Population Structure and Genome-Wide Signals of Positive Selection in South Asia. Am J Hum Genet. 2011 Dec;89(6):731–44. doi:10.1016/j.ajhg.2011.11.010

13 Supplementary Material

Table S1. Granular subject-level non-linear spatial normalization metrics across candidate template configurations (Kazakh, MNI152, and CN200).

subject	template	mean_u	std_u	mean_logJ	std_logJ	DSC	NCC
AKZ03_final	Kazakh	2.347069025	1.229276538	-0.01668957062	0.3171343505	0.9946695659	0.9907391071
AKZ03_final	MNI152	7.815505981	5.765951633	0.001659420435	0.3997235298	0.8759729437	0.6939541698
AKZ03_final	CN200	2.667143345	1.444813609	-0.03767009825	0.3519461155	0.9891220545	0.9767031074
AKZ05_final	Kazakh	2.303541899	1.178542614	-0.0319506675	0.2918225825	0.9946498773	0.9914889336
AKZ05_final	MNI152	5.158777237	4.589198112	-0.3584349453	0.4626222849	0.8116947754	0.5646428466
AKZ05_final	CN200	2.760537148	1.427599072	-0.05647657812	0.3390879631	0.9884253671	0.9777057767
AKZ06_final	Kazakh	2.300861597	1.221293449	-0.03387233615	0.3166952431	0.993884973	0.9877277613
AKZ06_final	MNI152	4.983448505	4.491571426	-0.3313779235	0.4408464432	0.7977893784	0.5482913256
AKZ06_final	CN200	2.878000259	1.411348104	-0.06393247098	0.3621035814	0.9876082427	0.9802981019
AKZ07_final	Kazakh	2.423218012	1.414172888	-0.01410268899	0.3137057424	0.9943700165	0.9898734093
AKZ07_final	MNI152	5.993284225	4.606036186	-0.3694203794	0.4436634481	0.8232901798	0.588204205
AKZ07_final	CN200	3.233119011	1.744769573	-0.04452138767	0.3552156687	0.988616077	0.9768466353
AKZ100_final	Kazakh	3.170671463	1.593919635	-0.05190709233	0.34996894	0.99319296	0.9863322973
AKZ100_final	MNI152	7.2660923	5.565150738	-0.01425608899	0.4017698467	0.8507110108	0.6726503372
AKZ100_final	CN200	3.909819365	1.772477269	-0.07903356105	0.3912846446	0.9862558158	0.9810260534
AKZ101_final	Kazakh	2.670407772	1.376670003	-0.02108222246	0.3059036136	0.9946125792	0.9900836945
AKZ101_final	MNI152	5.162945271	4.325049877	-0.3313153982	0.4294717312	0.8101689534	0.5657675266
AKZ101_final	CN200	3.014901876	1.615312576	-0.04982111603	0.3450837135	0.9890397823	0.9816437364
AKZ102_final	Kazakh	2.603568316	1.326074839	-0.03164561465	0.3186012805	0.9948848888	0.9907899499
AKZ102_final	MNI152	4.739584923	4.036606789	-0.3125965297	0.4269622862	0.8053620016	0.5587764978
AKZ102_final	CN200	2.918587923	1.57314539	-0.04739923403	0.3492466211	0.9887130241	0.97957623

AKZ105_final	Kazakh	2.322161674	1.147464275	-0.02064317279	0.3205787838	0.9949834684	0.9911951423
AKZ105_final	MNI152	7.913664341	5.705793858	-0.01398555096	0.4266071618	0.8656606451	0.6921330094
AKZ105_final	CN200	2.88830471	1.489306092	-0.04710501432	0.3505005538	0.9887320236	0.9810519218
AKZ106_final	Kazakh	2.551636696	1.350333333	-0.02458139695	0.3254061043	0.9948814581	0.9909034371
AKZ106_final	MNI152	5.657031059	4.591223717	-0.3668198287	0.4413171113	0.8213658044	0.5829994678
AKZ106_final	CN200	2.833589792	1.579965711	-0.04417219013	0.3308568001	0.9887059072	0.978491962
AKZ108_final	Kazakh	2.925373316	1.684289336	-0.02526517026	0.3213493228	0.9945153785	0.9905411005
AKZ108_final	MNI152	7.507133007	5.693717003	-0.0003384714364	0.3918987811	0.8647766663	0.6827622056
AKZ108_final	CN200	2.931342602	1.626737952	-0.04275852442	0.3371073008	0.9887281932	0.9786891341
AKZ113_final	Kazakh	2.762191057	1.782473922	-0.006484444253	0.3567770123	0.9917832536	0.984962821
AKZ113_final	MNI152	6.796384811	4.998961926	0.00646390114	0.383880347	0.833168531	0.6082785726
AKZ113_final	CN200	3.502497911	1.872344375	-0.03133627027	0.3870354593	0.9861656	0.9739199281
AKZ114_final	Kazakh	3.310874462	1.728630543	-0.1006249264	0.3703128695	0.9882392104	0.9757031798
AKZ114_final	MNI152	6.919261456	5.088126183	-0.05410636961	0.4063661993	0.8326804691	0.6356772184
AKZ114_final	CN200	4.288072586	2.070572615	-0.1354670525	0.4144636393	0.9745642314	0.9709133506
AKZ115_final	Kazakh	2.198452473	1.136850357	-0.02838411741	0.2971940935	0.99502971	0.9902462363
AKZ115_final	MNI152	7.393761158	5.499420166	-0.01048489939	0.3998020887	0.8642187835	0.6860263348
AKZ115_final	CN200	2.896137476	1.474743366	-0.05777416378	0.3548134565	0.9896584076	0.9785113335
AKZ116_final	Kazakh	3.075825214	1.619607091	-0.0513371639	0.3364493549	0.9897625824	0.9818748236
AKZ116_final	MNI152	5.890963078	4.641403198	-0.02366146073	0.3553353846	0.8470751915	0.659866631
AKZ116_final	CN200	3.560127974	1.609038234	-0.08801847696	0.3767706752	0.9847789797	0.9778546691
AKZ118_final	Kazakh	3.592774391	2.070025444	-0.1371221095	0.4387649	0.9878582436	0.9636030793
AKZ118_final	MNI152	7.924678802	5.23216486	-0.07259430736	0.449100554	0.821103636	0.6275932193
AKZ118_final	CN200	4.551039696	2.17447567	-0.1653737873	0.4802558422	0.978095078	0.9645406008
AKZ16_final	Kazakh	3.885908842	2.133849382	-0.103946358	0.4110029936	0.9916493442	0.9814175963
AKZ16_final	MNI152	7.401359081	4.881250858	-0.04292906076	0.4288980961	0.8401151628	0.6484459639
AKZ16_final	CN200	5.192995548	2.50204277	-0.1401818246	0.4813258946	0.9808661349	0.9681688547
AKZ17_final	Kazakh	3.652777433	1.685341358	-0.06195277721	0.4082378149	0.9904364083	0.9729216099
AKZ17_final	MNI152	6.899786949	4.590548992	-0.04778291285	0.3854229748	0.8378091528	0.6559081674
AKZ17_final	CN200	4.556121826	1.95537293	-0.05144520849	0.4351887107	0.9785919311	0.9663022757
AKZ18_final	Kazakh	2.561841965	1.425357819	-0.01740985736	0.3153650463	0.9944680181	0.9873489738
AKZ18_final	MNI152	6.948889256	5.163011074	-0.008700190112	0.3854559362	0.8542911261	0.6669066548
AKZ18_final	CN200	3.452087879	1.793539643	-0.04416960478	0.3461510539	0.9886389395	0.9786314964
AKZ20_final	Kazakh	2.86491251	1.449226022	-0.02967326529	0.3275128603	0.9933447573	0.9910647869
AKZ20_final	MNI152	5.157324314	4.385732651	-0.3368735313	0.4384060204	0.8054078555	0.5639676452

AKZ20_final	CN200	3.203842163	1.660064578	-0.07304081321	0.3607105017	0.9871573234	0.9781327248
AKZ21_final	Kazakh	2.491798639	1.195250511	-0.02385895327	0.2986263633	0.995015548	0.992125392
AKZ21_final	MNI152	6.882537365	5.028215408	-0.00429232046	0.3850392103	0.8593631025	0.672416985
AKZ21_final	CN200	3.212330818	1.542014122	-0.04736292362	0.3548689187	0.9890259247	0.9808445573
AKZ22_final	Kazakh	2.566156149	1.402437329	-0.02722960524	0.3057541251	0.9940190033	0.9896448255
AKZ22_final	MNI152	5.189554691	4.552384377	-0.3658057153	0.4639544189	0.8116773115	0.5668424368
AKZ22_final	CN200	2.863449574	1.422036171	-0.05175548047	0.3370358646	0.9879183541	0.9784355164
AKZ23_final	Kazakh	2.852030516	1.662797451	-0.02329765446	0.3272101581	0.9952424596	0.991227746
AKZ23_final	MNI152	8.150484085	5.988375664	-0.009662405588	0.4150449634	0.8611881889	0.6711390018
AKZ23_final	CN200	3.316686153	1.944450021	-0.04505821317	0.3405549824	0.9887744567	0.979347229
AKZ24_final	Kazakh	2.569165707	1.391014695	-0.0249096863	0.3086366951	0.9947743036	0.9908274412
AKZ24_final	MNI152	6.186891556	4.586699963	0.003598978044	0.3622644842	0.8539685867	0.6568630934
AKZ24_final	CN200	3.341338396	1.82714951	-0.06699327379	0.3610285819	0.9881423269	0.9799305201
AKZ32_final	Kazakh	2.172487259	1.109382391	-0.02891811728	0.3018128276	0.9939113318	0.9884662628
AKZ32_final	MNI152	6.591664791	5.501069069	-0.006372702308	0.3778945804	0.8545547307	0.6678447723
AKZ32_final	CN200	2.807009935	1.37408483	-0.05045450106	0.3289099932	0.9869716219	0.9783139825
AKZ34_final	Kazakh	2.529840231	1.371509552	-0.02803395689	0.2990724742	0.9953270631	0.9915542603
AKZ34_final	MNI152	5.352612972	4.417757034	-0.359051764	0.4350208938	0.8188205732	0.5834488869
AKZ34_final	CN200	3.122034311	1.601020932	-0.05704280734	0.3432329595	0.9889957113	0.9814915061
AKZ35_final	Kazakh	2.899096966	1.56172359	-0.03838879988	0.3459502161	0.9938816684	0.9861513376
AKZ35_final	MNI152	5.493993282	4.327429771	-0.3378686905	0.4396397769	0.7918897669	0.550950408
AKZ35_final	CN200	4.109455109	1.863083124	-0.07977999002	0.4023902714	0.987916432	0.9786628485
AKZ37_final	Kazakh	2.893619776	1.54105413	-0.02289578691	0.334798187	0.9950825301	0.9910811186
AKZ37_final	MNI152	6.892494678	5.524691105	0.01336912997	0.3614018261	0.8671816066	0.6808566451
AKZ37_final	CN200	3.51192522	1.763217688	-0.05494081229	0.3803313971	0.9890866474	0.979142487
AKZ38_final	Kazakh	3.046505451	2.366021395	0.04351842776	0.3567838967	0.9923278763	0.9752778411
AKZ38_final	MNI152	4.007811546	3.353121996	-0.2432237417	0.4117562175	0.8046007073	0.5819373131
AKZ38_final	CN200	3.351806641	2.026989698	0.001860354678	0.3877778947	0.9870487771	0.9596295357
AKZ42_final	Kazakh	2.505566359	1.345356703	-0.03581175953	0.3097079992	0.9940215552	0.9884447455
AKZ42_final	MNI152	5.679852486	4.741645813	-0.3728896379	0.4626266062	0.8038405486	0.5678309202
AKZ42_final	CN200	3.135057926	1.392066717	-0.05758926272	0.3602849245	0.98717529	0.9800850749
AKZ43_final	Kazakh	2.838067055	1.567205191	-0.04713602737	0.3353991807	0.994620297	0.9860801101
AKZ43_final	MNI152	6.560506344	4.73004961	-0.02911971882	0.3904812038	0.8505434962	0.666677773
AKZ43_final	CN200	3.43437314	1.943114281	-0.0647174269	0.3595663905	0.9882775932	0.97988832
AKZ44_final	Kazakh	2.596103191	1.340985537	-0.01711275987	0.3062450588	0.9950664285	0.991900444

AKZ44_final	MNI152	5.435760498	4.238014698	-0.3457959592	0.4330667257	0.8283787503	0.5961657166
AKZ44_final	CN200	3.234057426	1.609330654	-0.03410830349	0.3337500989	0.9890439953	0.9799672961
AKZ47_final	Kazakh	2.201785326	1.168494821	-0.0206253659	0.2975681722	0.9948046899	0.9910378456
AKZ47_final	MNI152	4.872147083	4.16808176	-0.3188296258	0.4254926145	0.8032661889	0.558259666
AKZ47_final	CN200	2.636384249	1.335495591	-0.0440823324	0.3220437765	0.9884653511	0.9804922342
AKZ50_final	Kazakh	2.56677413	1.445869327	-0.04078320786	0.3296051025	0.9942209555	0.9883083105
AKZ50_final	MNI152	7.734003067	5.758288383	-0.01873094589	0.4241274893	0.8558976348	0.676731348
AKZ50_final	CN200	3.204758883	1.602397323	-0.05524678528	0.3617343009	0.986808244	0.9773595333
AKZ54_final	Kazakh	2.508716822	1.421844363	-0.009849115275	0.3187618554	0.9949639587	0.9905641675
AKZ54_final	MNI152	5.617460728	4.425525665	-0.3582152724	0.4389709234	0.8226992737	0.588552177
AKZ54_final	CN200	3.094945431	1.477270246	-0.04873879999	0.3598043025	0.9895686296	0.9793023467
AKZ55_final	Kazakh	2.391205072	1.217955828	-0.02639072947	0.3147437871	0.994454544	0.9895886183
AKZ55_final	MNI152	4.947039127	4.126485825	-0.3345590234	0.4555068016	0.8090741793	0.5673840642
AKZ55_final	CN200	2.982424498	1.55121839	-0.0552345477	0.3606625497	0.9889914991	0.9790036678
AKZ58_final	Kazakh	2.719222784	1.422752142	-0.03298942	0.3213673532	0.9950227019	0.9904790521
AKZ58_final	MNI152	5.265984535	4.299852371	-0.3574727774	0.4793252945	0.8141724985	0.5795305967
AKZ58_final	CN200	2.987939358	1.490160584	-0.06226792186	0.3545525372	0.9894181307	0.9792206883
AKZ59_final	Kazakh	2.201411486	1.113946199	-0.02385934256	0.2966682911	0.9946621354	0.9908230901
AKZ59_final	MNI152	5.375586033	4.539291859	-0.3571313024	0.448621124	0.8077978992	0.5705634356
AKZ59_final	CN200	2.87245965	1.595330119	-0.0545809418	0.3513835967	0.9885475841	0.9812125564
AKZ62_final	Kazakh	2.604218006	1.232870221	-0.02663259022	0.3152573407	0.9946889064	0.9890732765
AKZ62_final	MNI152	8.112605095	6.203855038	-0.004792254884	0.4056307673	0.8564110755	0.6784288287
AKZ62_final	CN200	3.341599226	1.52955246	-0.06788987666	0.3639984131	0.9885085356	0.9808259606
AKZ63_final	Kazakh	2.425499916	1.24448657	-0.01911375672	0.2914857566	0.9950314698	0.9915795922
AKZ63_final	MNI152	7.552202702	5.825711727	0.001558105927	0.4063460231	0.8601026812	0.6795696616
AKZ63_final	CN200	3.093602896	1.567951322	-0.05630675331	0.345035404	0.9888879614	0.9811739922
AKZ64_final	Kazakh	2.432347059	1.245419502	-0.02217730507	0.2913670242	0.9950856089	0.9915836453
AKZ64_final	MNI152	6.970890045	5.289698601	0.004039577674	0.3861453831	0.8589712739	0.6761834025
AKZ64_final	CN200	3.08136797	1.574499488	-0.05835087225	0.346686393	0.9889168096	0.9812639356
AKZ67_final	Kazakh	2.72756505	1.380553007	-0.01652042754	0.3135277331	0.9950199133	0.991564095
AKZ67_final	MNI152	7.426587582	5.520947933	-0.004086385481	0.4033207893	0.8635050387	0.6665860415
AKZ67_final	CN200	3.232103109	1.634343743	-0.03899085522	0.3397952616	0.9882735554	0.9777514935
AKZ69_final	Kazakh	2.493590593	1.423619747	-0.03210320696	0.3443935812	0.9917156532	0.9834875464
AKZ69_final	MNI152	4.711791992	3.714356184	-0.3048821986	0.4320949316	0.799687618	0.5640597939
AKZ69_final	CN200	3.34533906	1.592089295	-0.06488591433	0.3742086589	0.9859786235	0.9718558788

AKZ71_final	Kazakh	2.423494339	1.252173662	-0.03958150744	0.3187881112	0.9942060798	0.9888553023
AKZ71_final	MNI152	5.483507633	4.412261009	-0.3639166057	0.44456774	0.8148731945	0.5777226686
AKZ71_final	CN200	2.915686846	1.440350652	-0.0623373203	0.3475830555	0.9877829115	0.9777514935
AKZ72_final	Kazakh	2.401744843	1.185754299	-0.03726799786	0.310307622	0.9946131068	0.9904382229
AKZ72_final	MNI152	5.631550789	4.554514408	-0.3679682314	0.4371965528	0.8249939227	0.600274086
AKZ72_final	CN200	2.945064783	1.496031284	-0.05527457222	0.3385798037	0.9880871056	0.9809744954
AKZ74_final	Kazakh	2.503994465	1.416615963	-0.01800349541	0.2968566418	0.9946911142	0.9907087684
AKZ74_final	MNI152	5.050149918	4.369695187	-0.3306751847	0.4313412011	0.8093784781	0.5688591003
AKZ74_final	CN200	3.028573036	1.592039704	-0.04876982048	0.3375274539	0.9887263149	0.9801973104
AKZ76_final	Kazakh	2.700340271	1.405987144	-0.06238858029	0.3507205844	0.9919837326	0.9811887145
AKZ76_final	MNI152	5.823156357	4.605476379	-0.02758879028	0.392039746	0.8418377319	0.6453953981
AKZ76_final	CN200	3.558398008	1.753557801	-0.08420959115	0.3799087405	0.9813975899	0.9721555114
AKZ78_final	Kazakh	2.454658985	1.262307644	-0.01450641733	0.3005390465	0.9951535914	0.9909647107
AKZ78_final	MNI152	5.541305542	4.423779011	-0.3763643205	0.4780703485	0.8232273126	0.5894383788
AKZ78_final	CN200	2.972146511	1.414218187	-0.05267458782	0.3565851152	0.9893360582	0.9822895527
AKZ81_final	Kazakh	2.335048199	1.207882524	-0.04767338187	0.3149213493	0.9949283659	0.988599956
AKZ81_final	MNI152	6.185709	5.006588459	-0.3979188502	0.4564853609	0.821175628	0.587587893
AKZ81_final	CN200	2.908851624	1.442089677	-0.06351155043	0.3512112796	0.9892166455	0.9784997106
AKZ84_final	Kazakh	2.519846916	1.301037908	-0.01894954406	0.3119409084	0.9946833769	0.9894060493
AKZ84_final	MNI152	6.471190453	4.858261585	-0.01325622853	0.3939341009	0.8685918944	0.6850178838
AKZ84_final	CN200	3.248910427	1.672307491	-0.04749542102	0.3544722497	0.9888215809	0.9796010852
AKZ85_final	Kazakh	2.444059372	1.254691601	-0.04347201809	0.3109390438	0.9946171756	0.9894764423
AKZ85_final	MNI152	5.440163612	4.570161819	-0.3522083461	0.452514708	0.8058072392	0.5589312911
AKZ85_final	CN200	3.380088568	1.917442679	-0.06464412063	0.3599004745	0.9883463374	0.9799121022
AKZ88_final	Kazakh	2.427913904	1.2372756	-0.02582903393	0.294968307	0.994766479	0.9911820292
AKZ88_final	MNI152	7.7227211	5.724609852	-0.01818618178	0.4225075245	0.8623329006	0.6863588691
AKZ88_final	CN200	2.818532228	1.513981581	-0.04628583044	0.3309988379	0.988734654	0.9805166125
AKZ89_final	Kazakh	2.793134928	1.426247597	-0.04900738969	0.3291209042	0.9931571284	0.9848048091
AKZ89_final	MNI152	5.217336655	4.37857008	-0.3488864005	0.4665327668	0.7922041325	0.5504217744
AKZ89_final	CN200	3.5727005	1.761204004	-0.07677389681	0.3769733906	0.9853418986	0.976929605
AKZ90_final	Kazakh	2.55811882	1.482433915	-0.01633234881	0.3241491914	0.9951044266	0.9917376637
AKZ90_final	MNI152	6.002403259	4.819322109	-0.3892907798	0.489636451	0.8284286588	0.5982382894
AKZ90_final	CN200	3.112870693	1.629763246	-0.03534675017	0.3562738001	0.9890450201	0.9789179564
AKZ94_final	Kazakh	2.307867527	1.238137603	-0.009058185853	0.3005872965	0.9949114743	0.9911248684
AKZ94_final	MNI152	5.956896782	4.565507412	-0.3594952822	0.4338735044	0.8278274971	0.6024542451

AKZ94_final	CN200	3.003562689	1.502536416	-0.02767485008	0.3346075118	0.9891731718	0.9817499518
AKZ95_final	Kazakh	2.550483465	1.243400812	-0.04978802055	0.329901129	0.9920692499	0.9820674062
AKZ95_final	MNI152	5.151266098	4.247384548	-0.352480948	0.4703045487	0.7927936251	0.5550462008
AKZ95_final	CN200	3.307732821	1.514252543	-0.0792799294	0.3777007461	0.9850092691	0.9778436422
AKZ96_final	Kazakh	2.485742092	1.37212348	-0.0328213647	0.3163208067	0.9918220562	0.9849084616
AKZ96_final	MNI152	5.738529205	4.768037796	-0.3970698416	0.4919025004	0.8121076604	0.5883660316
AKZ96_final	CN200	2.976420641	1.607312799	-0.0804335624	0.3708917499	0.9858874986	0.9798721671
AKZ97_final	Kazakh	2.530930758	1.345754504	-0.02736330032	0.323533386	0.9934951673	0.9859236479
AKZ97_final	MNI152	7.930301189	6.197316647	-0.00341122644	0.3995561302	0.8526860655	0.6726082563
AKZ97_final	CN200	3.243790627	1.513281822	-0.07693465054	0.3815091252	0.9872533068	0.9800174832
AKZ99_final	Kazakh	2.330645323	1.210847855	-0.03018486314	0.2975040674	0.9945993565	0.9892670512
AKZ99_final	MNI152	5.213595867	4.598991871	-0.3390575051	0.4350173175	0.8060552534	0.5646277666
AKZ99_final	CN200	2.696291685	1.435359716	-0.05316161364	0.3305657208	0.9885709815	0.978575050

755

Supplementary Files

This is a list of supplementary files associated with this preprint. Click to download.

- loocvresults.pdf